Appl Phys B (2010) 98: 337–346
DOI 10.1007/s00340-009-3759-6

Applied Physics B
Lasers and Optics

Optical spectra and luminescence dynamics of the Dy-doped Gd_2SiO_5 single crystal

R. Lisiecki · G. Dominiak-Dzik · P. Solarz · W. Ryba-Romanowski · M. Berkowski · M. Głowacki

Received: 20 May 2009 / Revised version: 2 September 2009 / Published online: 2 October 2009

Abstract Spectroscopic properties of the Dy^{3+}:Gd_2SiO_5 (GSO) single crystal were investigated. The polarized absorption and unpolarized emission spectra were measured at temperature ranging from 10 K to 300 K. Experimental oscillator strengths were determined from room temperature polarized absorption spectra and phenomenological intensity parameters Ω_t were calculated by using the standard Judd–Ofelt theory. Low-temperature measurements were used to determine the energy level structure of two nonequivalent Dy^{3+} sites in the GSO crystalline host. Analysis of spectra and decay curves of the $^4F_{9/2}$ emission revealed that Dy^{3+} ions entering nine-coordinated sites with C_{3v} symmetry and Dy^{3+} ions entering the seven-coordinated sites with C_s symmetry form two distinct, well-isolated subsystems weakly coupled by the spectral energy migration process. In addition to dissimilar crystal field splitting of multiplets, the two subsystems differ significantly in the efficiency of excitation energy transfer between dysprosium ions, thereby showing dissimilar self-quenching of the $^4F_{9/2}$ emission. Besides, only one of the two Dy^{3+} subsystems is coupled to Gd^{3+} ions by nonradiative Gd^{3+}–Dy^{3+} energy transfer process. Laser potential related to the $^4F_{9/2} \rightarrow {}^6H_{13/2}$ yellow luminescence of dysprosium ions was assessed based on evaluation of the emission cross-section values. It was concluded that the Dy:Gd_2SiO_5 (Dy:GSO) is a promising material for the visible laser operation.

R. Lisiecki (✉) · G. Dominiak-Dzik · P. Solarz · W. Ryba-Romanowski
Institute of Low Temperature and Structure Research, Polish Academy of Sciences, Wrocław, Poland
e-mail: R.Lisiecki@int.pan.wroc.pl
Fax: +48-71-3441029

M. Berkowski · M. Głowacki
Institute of Physics, Polish Academy of Sciences, Warsaw, Poland

PACS 42.55.Xi · 42.62.Fi

1 Introduction

Literature concerning optical properties of dysprosium-doped matrices is by far less exhausting as compared to other rare earth ions. In early works, the main interest was directed to feasibility of laser operation associated with the $^6H_{13/2} \rightarrow {}^6H_{15/2}$ transition of Dy^{3+} near 3 μm. It has been then realized that to maintain high quantum efficiency of the $^6H_{13/2}$ upper laser level, the choice of host matrices is restricted essentially to fluoride or chloride crystals and glasses which display low-energy lattice vibrations thereby reducing the rate of multiphonon relaxation. Such a requirement was not encouraging since the manufacture technology of fluoride compounds is more demanding than the preparation of oxide compounds. As a consequence, the report on laser performance at 3.022 μm of BaY_2F_8:Dy^{3+} [1], published in the 1970s, was not followed for a long time by further studies in this topic. In a more recent paper [2] the laser potential associated with the $^6F_{5/2}$–$^6H_{11/2}$ transition at 1.55 μm in dysprosium-doped $CsCdBr_3$ and KPb_2Cl_5 crystals has been examined. The growing interest in the visible luminescence of Dy^{3+} is stimulated by practical reasons. The occurrence of two intense luminescent transitions near 480 nm (blue emission) and near 570 nm (yellow emission) is promising for application as a white-light emitting phosphor [3, 4]. Also, the design of visible lasers employing dysprosium-doped matrices seems to be the most tempting issue owing to a highly efficient luminescence in the visible. Moreover, an intense yellow emission offers the potential of laser operation in the four-level scheme since the related transition terminates in the $^6H_{13/2}$ level which is situated well above the ground $^6H_{15/2}$ level ($\Delta E = 3600\ cm^{-1}$).

In spite of these advantages, dysprosium-doped materials were not considered as promising visible lasers because low absorption cross-section of bands between the upper laser level and the UV absorption edge of hosts could hardly provide sufficient absorption efficiency upon lamp pumping. However, a spectacular progress in the development of blue-emitting semiconductor lasers would supply a remedy for poor efficiency of optical pumping in this range. It has been reported that the gadolinium oxyorthosilicate Gd_2SiO_5 crystal doped with Ce^{3+} is promising scintillator, especially for medical and nuclear physics applications [5]. It was shown that the Eu:Gd_2SiO_5 crystal can be promising candidate for the VUV-excited phosphor owing to the efficient energy transfer from Gd^{3+} or host to Eu^{3+} [6]. It was reported also that GSO doped with Yb^{3+} can be a promising material for potential laser action [7].

In this work we report results of optical investigation of trivalent dysprosium in the Gd_2SiO_5 single crystal grown by the Czochralski technique. Polarized absorption spectra, luminescence, and excited state dynamics were investigated at 10–300 K. Energies of crystal-field components were determined based on low-temperature optical spectra. Particular attention was directed to spectroscopic features relevant to potential visible laser operation. Emission-cross sections were determined for yellow luminescence at around 570 nm.

2 Optical technique

The Gd_2SiO_5:Dy^{3+} crystals were grown in Institute of Physics, PAS, Warsaw, using the Czochralski method. Polarized absorption spectra were measured at 10 and 300 K with a Varian model 5E UV-VIS-NIR spectrophotometer. The resolution was 0.05 nm in the UV-VIS region and 0.1 nm in the NIR. Luminescence was recorded with a set-up consisting of Dongwoo Optron DM 711 and DM 158i monochromators with 750 and 150 mm focal range, respectively and the Hamamatsu 955 photomultiplier. The ozone-free Xenon Lamp DL 80-Xe and an Argon ion laser were used as excitation sources. The temperature of samples were varied between 10 and 300 K. Luminescence decay curves were recorded with a Tektronix TDS 3052 digital oscilloscope following selective sample excitation by a Continuum Surelite 1 optical parametric oscillator (OPO) pumped by a third harmonic of an Nd:YAG laser with 4-ns pulse. The measurements were carried out within the 10–300 K temperature range. The continuous flow liquid–helium cryostat (Oxford Instruments) was used in low-temperature measurements.

3 Results and discussions

3.1 Crystal growth and crystal structure

Single crystals of gadolinium orthosilicate $(Gd_{1-x}Dy_x)_2SiO_5$ with $x = 0.01$ and 0.05 were grown by the Czochralski method in inductively heated iridium crucible under nitrogen atmosphere. The starting materials of 99.99% purity were used. They were fired at 1000°C for 4 hours before weighing and mixing. A stoichiometric mixture of Gd_2O_3 and SiO_2 powders was used, as starting materials, in a molar ratio of 1:1. The admixture of dysprosium was doped into above mixture at the content of 1 and 5 mol% in place of gadolinium. These materials were put together and then pressed into cylinder tablets under high pressure. The tablets were sintered in a furnace at the temperature of 1500°C for 6 hours before they were loaded into a crucible. Single crystals were grown with convex crystal melt interface on an iridium 2 mm rod with pulling rate of 1.5–2 mm/h and speed of rotation 20 rpm. Transparent and almost colorless crystals (crystals with 5% of Dy have light green–yellow color) with strong tendency to cracking parallel to the cleavage plane (100) with 20 mm of diameter were grown from 40 mm crucible.

The chemical analysis has been carried out for *as-grown* single crystals with Inductively Coupled Plasma (ICP) instrument. The obtained concentration of dysprosium in crystals amounting to 0.98 ± 0.01 and 4.95 ± 0.01 at% for $x = 0.01$ and $x = 0.05$, respectively, indicates that the effective segregation coefficient k_{eff} is slightly lower than unity.

The structure of GSO:Dy was investigated at room temperature by means of the precise powder X-ray diffraction method using a Siemens D5000 diffractometer with filtered CuKα radiation and scintillation counter as a detector. The diffraction patterns were measured with a step of 0.02° and an averaging time of 10 s/step. The experimental data were analyzed by the Rietveld refinement method using the R.A. Young DBWS-9807 package [8] that enabled us to take into account positional and thermal corrections, scaling factor, zero shift, background parameter, Bragg-peak profile parameter, and extinction correction. The Gd_2SiO_5 crystal is a monoclinic system with a $P2_1/c$ space group. The determined lattice parameters, $a = 9.1105$ Å, $b = 6.9783$ Å, $c = 6.8544$ Å, $\beta = 107.1411$, and $V = 416.42$ Å^3 are consistent with data reported in reference [9]. The plates with orientation (010) and (100) were cut from the GSO:Dy 1% and GSO:Dy 5% crystal boules, respectively, and used in our optical experiments. The photographs of the Dy:GSO *as-grown* crystal and prepared polished samples are presented in Fig. 1. In the GSO crystal, Gd^{3+} ions occupy two non-equivalent crystallographic sites, the Gd1 sites with coordination number CN = 9 and Gd2 site with CN = 7. The site notation used by us is this work is consistent with crystallographic data. The point symmetry of Gd1 and Gd2 sites is C_{3v} and C_s, respectively. Figure 2 shows coordination polyhedra of Gd1 and Gd2 and the crystal structure of the GSO crystal in the *ab* projection. All oxygen atoms create bonds to silicon (silicon-bonded atoms) except for the O5 ones that join gadolinium atoms. Three non-silicon-bonded atoms

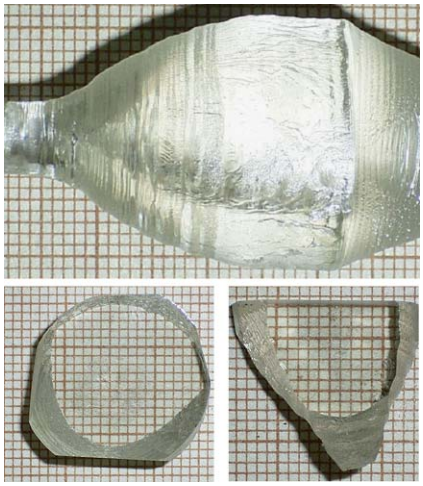

Fig. 1 The as-grown Gd_2SiO_5 crystal

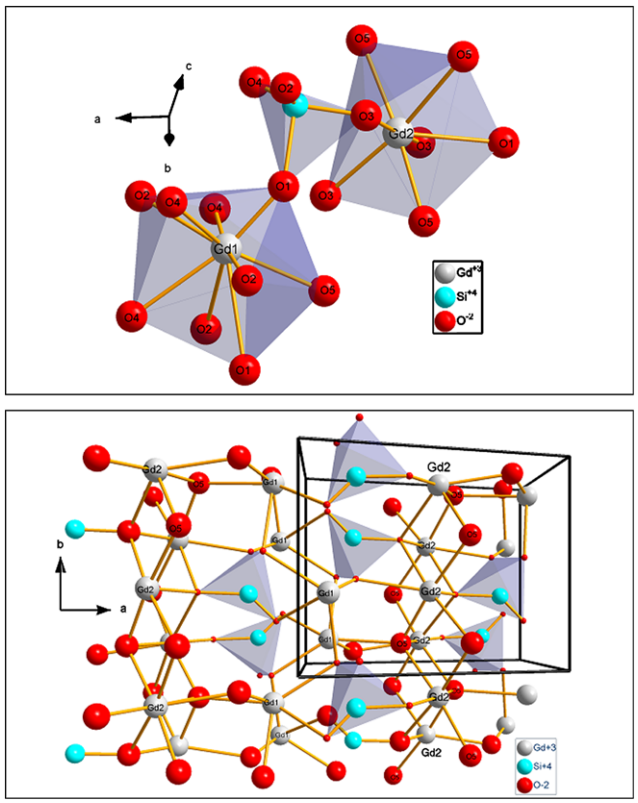

Fig. 2 Symmetry of the closest vicinity of gadolinium ions in the Gd_2SiO_5 structure

(O5) around Gd2 create shorter bonds (2.295, 2.300, and 2.303 Å) than one O5 atom around Gd1 (2.351 Å). Moreover, Gd2 ions create nearly linear chains along crystallographic *b* axis. The Gd2–Gd2 distance of 3.499 Å is much shorter than the distances between Gd2–Gd1 (3.781 Å) and Gd1–Gd1 (3.734 Å). Selected interatomic distances are presented in Table 1. It seems that Dy^{3+} ions, like Ce^{3+}, Eu^{3+}, Er^{3+}, or Yb^{3+} ions [5–7, 9, 10], will substitute both Gd1 and Gd2 sites of Gd_2SiO_5.

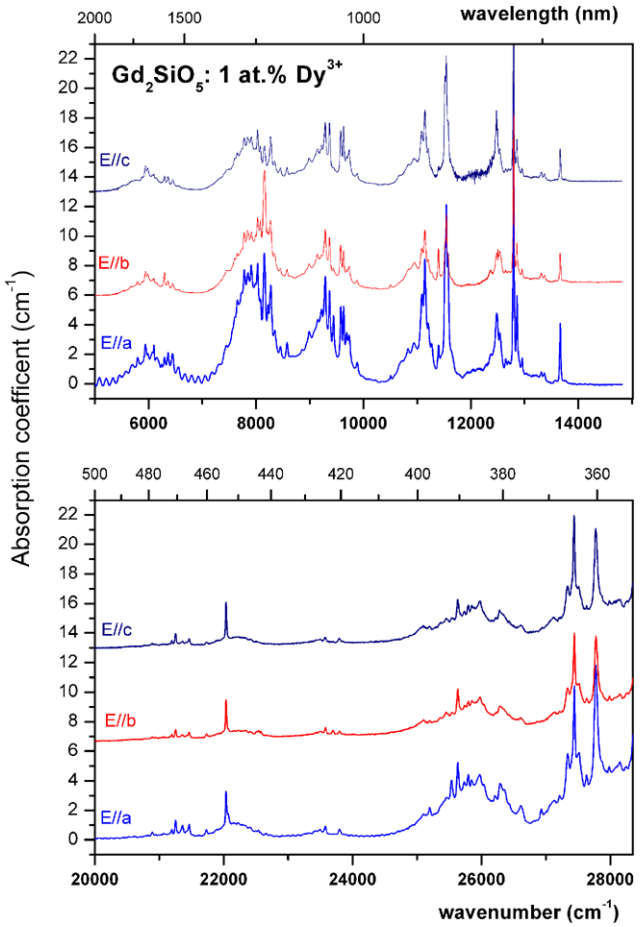

Fig. 3 Polarized absorption spectrum of Dy^{3+} ions in the Gd_2SiO_5 crystal recorded at 300 K

3.2 Transition intensities

Figure 3 shows room-temperature absorption spectra of GSO:Dy measured with an incident light polarized parallel to the *a*, *b*, and *c* crystallographic axes. The considered transitions are electric dipole in character. The $^6H_{15/2} \rightarrow {}^6H_{13/2}$ magnetic dipole transition at ~3700 cm^{-1} was not acquired in absorption. Based on these spectra, experimental oscillator strengths of nine bands have been determined according to following equation:

$$P_i^{\exp} = \frac{4.33 \times 10^{-9}}{d \times C} \int \alpha(\nu)\, d\nu, \quad (1)$$

where *i* denotes the status of light polarization and is related to *E*//*a*, *E*//*b*, *E*//*c* spectra. The $\int \alpha(\nu)\, d\nu$ means an integrated area under individual absorption band expressed in terms of absorption coefficient α at a wavenumber ν, *d* is the crystal thickness in cm, and *C* denotes a concentration

Table 1 Bond lengths of Gd1–O^{-2} and Gd2–O^{-2}, and minimal distances between Gd1 and Gd2 ions in the Gd_2SiO_5 crystal

Gd^{3+}–O^{-2} system with CN = 9		Bond lengths (Å)	Gd^{3+}–O^{-2} system with CN = 7		Bond lengths (Å)
Gd1	O1	2.272	Gd2	**O5**	**2.295**
	O2	2.337		**O5**	**2.300**
	O5	**2.351**		**O5**	**2.303**
	O4	2.412		O3	2.382
	O2	2.495		O1	2.399
	O1	2.510		O3	2.502
	O2	2.557		O3	2.532
	O4	2.689			
	O4	2.761			

Minimal Gd^{3+}–Gd^{3+}		Distances (Å)
Gd2	Gd2	3.499
Gd1	Gd1	3.734
Gd1	Gd2	3.781

Table 2 Electric-dipole oscillator strengths of Dy^{3+} in Gd_2SiO_5

Transition from $^6H_{15/2}$	Energy (cm^{-1})	Oscillator strength P_i (10^{-6})					Residual
		$(E//a)$	$(E//b)$	$(E//c)$	P_{mean}	P_{calc}	$\lvert\Delta P\rvert$ (10^{-6})
$^6H_{11/2}$	6029	2.69	1.61	1.72	2.01	2.03	0.02
$^6H_{9/2}$, $^6F_{11/2}$	7889	7.02	6.55	4.31	5.96	5.99	0.03
$^6H_{7/2}$, $^6F_{9/2}$	9386	3.71	2.76	3.27	3.25	4.60	1.35
$^6H_{5/2}$, $^6F_{7/2}$	11145	4.88	3.33	4.13	4.12	3.99	0.13
$^6F_{5/2}$, $^5F_{3/2}$	13036	2.87	2.93	3.04	2.95	2.39	0.56
$^4F_{9/2}$	21168	0.36	0.16	0.29	0.27	0.32	0.05
$^4I_{15/2}$	22200	0.91	0.80	0.81	0.84	0.75	0.09
$^4G_{11/2}$	23569	0.36	0.29	0.30	0.29	0.10	0.19
Ω_t (10^{-20} cm^2):		$\Omega_2 = 3.22$		$\Omega_4 = 2.16$		$\Omega_6 = 3.76$	

of an optical impurity expressed in mol × cm^{-3}. Mean experimental oscillator strengths P_{mean} were calculated in the way

$$P_{mean} = \frac{1}{3}\sum_{i=a}^{c} P_i. \tag{2}$$

In the Judd–Ofelt theory the oscillator strength of an electric-dipole transition between initial state aJ and final state bJ' is expressed as

$$P_{cal} = \frac{8\pi^2 mc}{3h\lambda(2J+1)}\frac{(n^2+2)^2}{9n} \times \sum_{t=2,4,6} \Omega_t \left|\left\langle f^N[L,S]J\right|\left|U^{(t)}\right|\left|f^N[L',S']J'\right\rangle\right|^2, \tag{3}$$

where λ is the mean wavelength of the transition, n is the refractive index of the host ($n = 1.85$ [14]). The $U^{(t)}$ represent matrix elements of unit tensor $U^{(t)}$ [11, 12]. Symbols m, c, and h denote the electron mass, the light velocity, and the Planck constant, respectively. The values of experimental and calculated oscillator strengths are gathered in Table 2. The P_{exp} and P_{calc} are in a good agreement except for the $^6H_{15/2} \rightarrow (^6H_{7/2}, ^6F_{9/2})$ transition. The phenomenological intensity parameters, determined by a least-squares-fitting approach, are as follows: $\Omega_2 = 3.22$ (10^{-20} cm^2), $\Omega_4 = 2.16$ (10^{-20} cm^2), and $\Omega_6 = 3.76$ (10^{-20} cm^2). With the Ω_t parameters found, the radiative transition rates A_{rad} from the $^4F_{9/2}$ level to the ^6F_J and ^6H_J manifolds were calculated according to the relation

$$A_{rad} = \frac{64\pi^4 e^2}{3h(2J+1)\lambda^3}\frac{n(n^2+2)^2}{9} \times \sum_{t=2,4,6} \Omega_t \left|\langle bJ'|\left|U^{(t)}\right||aJ\rangle\right|^2. \tag{4}$$

The resulting values, together with luminescence branching ratios β and the $^4F_{9/2}$ radiative lifetime τ_{rad}, are reported

Table 3 Radiative transition rates A_{rad}, theoretical and experimental branching ratios β, and radiative lifetime τ_{rad} of the $^4F_{9/2}$ luminescence state in Dy:Gd_2SiO_5

$^4F_{9/2} \rightarrow {}^{2S+1}L_J$ emission	A_{rad} (s^{-1})	β_{theor}	β_{exp}
$^6H_{15/2}$	516	0.2798	0.35
$^6H_{13/2}$	1003	0.5435	0.58
$^6H_{11/2}$	76	0.0411	0.05
$^6H_{9/2}$	27	0.0145	0.02
$^6F_{11/2}$	30	0.0164	
$^6F_{9/2}$	13	0.0070	–
$^6H_{7/2}$	156	0.0845	–
$^6H_{5/2}$	7	0.0039	–
$^6F_{7/2}$	10	0.0054	–
$^6F_{5/2}$	7	0.0037	–
$^6F_{3/2}$	0.24	0.0002	–
$\sum A_{rad} = 1845\ s^{-1}$			
$\tau_{rad}\ (^4F_{9/2}) = 542\ \mu s$			

$\beta = \frac{A_{rad}}{\sum_j A_{rad}}$ and $\tau_{rad} = \frac{1}{\sum_j A_{rad}}$

in Table 3. According to the phenomenological model prediction, the major part of the $^4F_{9/2}$ excitation should be emitted to the $^6H_{13/2}$ first excited level (~55%) and to the $^6H_{15/2}$ ground state (~28%). It follows from the Table 3 that the experimental branching ratios β_{exp} ($^6H_{15/2}$ ~35%; $^6H_{13/2}$ ~58%;) determined by using the emission spectra are close to theoretical values β_{theor}. The $^4F_{9/2}$ radiative lifetime amounts to 542 µs and is comparable to radiative lifetime reported for the Dy:YAB system (572 µs) [4] and longer than these reported for Dy:$LiNbO_3$ (387 µs) [13] or (130 µs) Dy:YVO_4 [15].

3.3 Energy level structure of Dy^{3+}

Low-temperature absorption spectrum (Fig. 4a) and low-temperature emission spectra related to the $^4F_{9/2} \rightarrow {}^6H_{13/2}$ and $^4F_{9/2} \rightarrow {}^6H_{15/2}$ transitions (Fig. 4b, c) were used to determine the crystal-field level structure of Dy^{3+} in GSO matrix. Absorption bands recorded in the 5500–42 500 cm^{-1} spectral range correspond to intraconfigurational transitions within the $4f^9$ electronic configuration of Dy^{3+} except for intense lines in the UV region that correspond to gadolinium absorption: $^8S_{7/2} \rightarrow {}^6P_{7/2,5/2}$ (31 500–32 800 cm^{-1}) and $^8S_{7/2} \rightarrow {}^6I_J$, ^6D_J (35 500–41 500 cm^{-1}). The band assignments have been made on the basis of energy level scheme reported by Carnal et al. [11] and Jayasankar et al. [12].

Analysis of these low-temperature optical data revealed that the number of spectral lines in each optical band is greater than predicted for a single site of Dy^{3+} with given point symmetry. Hence, Dy^{3+} ions in the Gd_2SiO_5 matrix occupy both Gd1 and Gd2 sites. The 10 K absorption spectrum related to the $^6H_{15/2} \rightarrow {}^4F_{9/2}$ transition (Fig. 4c: inverted spectrum) contains ten well-resolved spectral lines consistent with transitions from the lowest crystal-field component of the ground multiplet to the $^4F_{9/2}$ multiplet of both dysprosium sites having five crystal-field components each. Assignment of these lines to individual Dy^{3+} sites cannot be inferred from absorption spectra, however. High-resolution site selective excitation would be helpful. Unfortunately, our attempts to excite selectively individual crystal-field components of Dy^{3+} multiplets were unsuccessful because of low spectral resolution of the excitation monochromator. Instead, examination of acquired data revealed that the luminescence spectra excited into Dy^{3+} multiplets differ significantly from those recorded upon excitation of Gd^{3+} followed by Gd^{3+}–Dy^{3+} energy transfer. It follows from Figs. 4b and 4c that the Dy^{3+} luminescence spectra excited at 312 nm into the $^6P_{7/2}$ multiplet of Gd^{3+} spectra are consistent with transitions of Dy^{3+} in one site only, whereas both the Dy^{3+} sites contribute to the emission spectrum excited at 360 nm into the Dy^{3+} multiplet. From these spectra the lowest crystal-field components of the $^4F_{9/2}$ level for the two Dy^{3+} sites were located at 21 094 and 21 195 cm^{-1}. In addition, these spectra made it possible to locate the crystal-field components of the terminal $^6H_{15/2}$ and $^6H_{13/2}$ multiplets. To determine the energies of remaining crystal-field components of the luminescent $^4F_{9/2}$ multiplet the luminescence spectra were recorded for the two excitation wavelengths at temperatures up to 300 K. The results of measurement are shown in Fig. 5. With increasing sample temperature, the higher energy components become thermally populated, and the corresponding lines appear in the spectra. The increase of the crystal temperature to $T \geq 50$ K leads to effective population of the $^4F_{9/2}$ crystal-field components, and successive lines located at short-wavelength part of spectrum are observed in emission. Emission lines at 21 256, 21 365, and 21 470 cm^{-1} have been identified as $^4F_{9/2}(1) \rightarrow {}^6H_{15/2}(0)$, $^4F_{9/2}(2) \rightarrow {}^6H_{15/2}(0)$, and $^4F_{9/2}(3) \rightarrow {}^6H_{15/2}(0)$ transitions, respectively. The $^4F_{9/2}(0) \rightarrow {}^6H_{15/2}(0)$ line occurs at 21 195 cm^{-1} at 10 K. In the $F_{9/2} \rightarrow {}^6H_{13/2}$ band, analogous lines occurs at 17 515 ($0 \rightarrow 0$), 17 572 ($1 \rightarrow 0$), 17 683 ($2 \rightarrow 0$), and 17 784 cm^{-1} ($3 \rightarrow 0$). These lines are marked in Fig. 5.

The derived number and energies of crystal-field components of Dy^{3+} multiplets in GSO are listed in Table 4. Worth mentioning is the fact that the overall crystal-field splitting of the $^6H_{15/2}$, $^6H_{13/2}$, and $^4F_{9/2}$ multiplets for the Dy^{3+} site denoted by Dy2 in Table 4 is markedly higher than for Dy1 site. Besides, the overall crystal field splitting of the ground $^6H_{15/2}$ multiplet for Dy2 site amounting to 922 cm^{-1} is unusually high. For a comparison, the corresponding reported values are 470 cm^{-1} for Dy:$YAl_3(BO_3)_4$ and 603 cm^{-1} for Dy:$LiNbO_3$ crystals [4, 13].

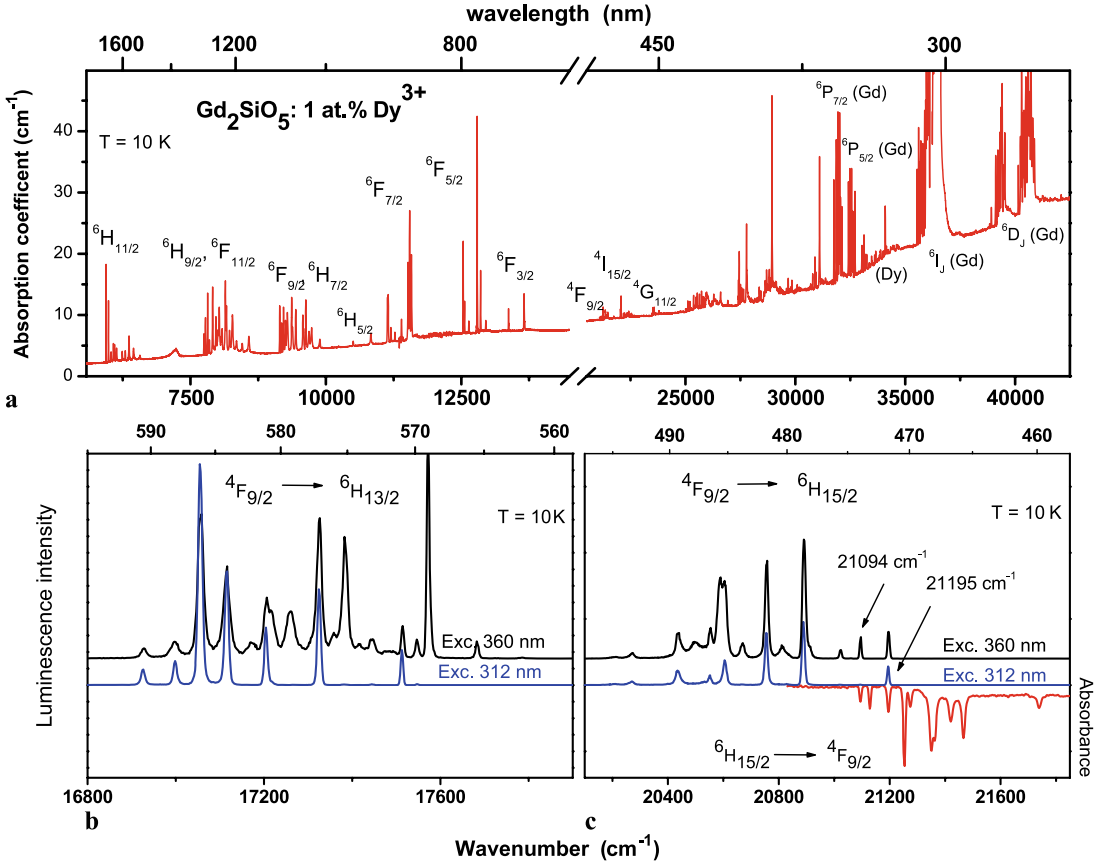

Fig. 4 Low-temperature optical spectra of Dy^{3+} ions in the Gd_2SiO_5 matrix. Panel (**a**) shows absorption of Dy^{3+} and Gd^{3+} ions; panels (**b**, **c**) correspond to the Dy^{3+} emissions acquired under the 312 and 360 excitation

The experimental results presented above imply that the two Dy^{3+} sites in GSO matrix are not connected by spectral energy migration, and they form isolated luminescence centers. In addition, only one of these two centers is strongly favored by the $Gd^{3+} \rightarrow Dy^{3+}$ energy transfer process.

Even though two sites of Dy^{3+} ions are unambiguously characterized by luminescence data, their identification is difficult owing to the low point symmetry of the each site. However, optical properties are determined by crystallographic structure. Thus, spectroscopic characteristics of Dy^{3+} sites can be correlated with microstructure of individual site. Considering differences in the Dy^{3+}–O^{2-} and Dy^{3+}–Dy^{3+} bond distances, the number of non-silicon-bonded atoms of oxygen, and the chain structure of Dy2 in the crystal structure, we presumed that energy transfer among Dy^{3+} ions should be more effective in the Dy2–Dy2 system than in the Dy1–Dy1 one.

3.4 Excited state relaxation dynamics

Under a weak excitation, the luminescence decay of an excited ion is governed by a sum of probabilities for several competing processes: radiative decay A_{rad}, nonradiative decay by multiphonon emission A_{mph}, and by nonradiative energy transfer A_{NET} to other ions. Thus, the experimental decay time is expressed as

$$\tau_{exp} = \frac{1}{A_{rad} + A_{mph} + A_{NET}}. \quad (5)$$

In the Gd_2SiO_5:Dy system the nonradiative decay by multiphonon emission from the $^4F_{9/2}$ state is expected to be small due to the large energy gap to the next lower $^6F_{1/2}$ ($\sim$13 800 cm^{-1}) as compared to the highest energy of phonons involved ($\sim$900 cm^{-1}) [10]. As many as eight phonons would be needed to cover the energy gap of 7300 cm^{-1}. Thus, radiative decay and nonradiative energy transfer among Dy^{3+} ions can influence of the $^4F_{9/2}$ lifetime. Figure 6 presents the semi-logarithmic plots of the $^4F_{9/2}$ experimental decays of the GSO crystal doped with 1 and 5 at% of Dy^{3+}. The luminescence decay curves were recorded at 10 K. The crystals were excited at 454 nm, and the spectral bandwidth of the excitation light pulses delivered by OPO was large enough (about 40 cm^{-1}) to excite simultaneously the two Dy^{3+} sites. The luminescence was acquired at different emission wavenumbers, 21 095 cm^{-1} and

Table 4 Energies of crystal-fields components of Dy^{3+} in Gd_2SiO_5

$^{(2S+1)}L_J$	Energy in cm^{-1}	Number of crystal-field components	
		Theoretical (in C_{3v} and C_s)	Observed
$^6H_{15/2}$	0, 306, 440, 590, 642, 758, 922 (Dy2) 0, 74, 184, 284, 426, 506, 598 (Dy1)	16	14
$^6H_{13/2}$	3682, 3870, 3991, 4080, 4140, 4196, 4269 (Dy2) 3547, 3649, 3712, 3822, 3875 (Dy1)	14	12
$^6H_{11/2}$	5942, 5987, 6035, 6080, 6100, 6136, 6241, 6260, 6297, 6367, 6449, 6567	12	12
$^6H_{9/2}$, $^6F_{11/2}$	7747, 7777, 7816, 7852, 7909, 7939, 7970, 7995, 8012, 8031, 8069, 8085, 8144, 8166, 8221, 8276, 8350, 8457, 8579	22	19
$^6H_{7/2}$, $^6F_{9/2}$	9147, 9181, 9218, 9254, 9278, 9288, 9298, 9368, 9173, 9444, 9531, 9547, 9589, 9630, 9688, 9737, 9889	18	17
$^6H_{5/2}$	10 237, 10 447, 10 504, 10 706, 10 832	6	5
$^6F_{7/2}$	11 138, 11 150, 11 200, 11 273, 11 394, 11 518, 11 547, 11 579	8	8
$^6F_{5/2}$	12 535, 12 560, 12 638, 12 792, 12 856, 12 951	6	6
$^6F_{3/2}$	13 371, 13 379, 13 658, 13 670	4	4
$^6F_{1/2}$	not observed	2	–
$^4F_{9/2}$	21 195, 21 254, 21 360, 21 463, 21 731 (Dy2) 21 094, 21 128, 21 274, 21 351, 21 420 (Dy1)	10	10
$^4I_{15/2}$	22 043, 22 070, 22 180, 22 227, 22 309, 22 333, 22 356, 22 419, 22 484, 22 502, 22 542, 22 581, 22 665	16	13
$^4G_{11/2}$	23 485, 23 515, 23 576, 23 609, 23 699, 23 795, 23 866	12	7

17 064 cm^{-1}. These emission wavenumbers were chosen since it follows from spectra in Figs. 4b and 4c that they correspond to emission lines of Dy1 and Dy2 sites, respectively. The $^4F_{9/2}$ luminescence collected at 21 095 cm^{-1} for the crystal with 1 at% of Dy^{3+} can be described by a single exponential function with a time constant of 514 µs. However, a slightly nonexponential and faster decay is observed when luminescence is monitored at 17 064 cm^{-1}. Such observation implies that the Dy2 site has a shorter lifetime (emission monitored at 17 064 cm^{-1}) than the Dy1 site (emission monitored at 21 095 cm^{-1}). Luminescence decay curve for Dy2 site deserves some more attention, however. It follows from Fig. 6 that it is not exponential in the initial stage of decay, but finally it approaches the exponential time dependence with the time constant amounting to 497 µs. Such a time dependence is typical for a luminescence decay involving the self-quenching of luminescence via cross-relaxation process when the excitation energy migration over donor ions does not occur. The initial nonexponential stage of the decay would thus correspond to the static quenching with the Forster-like time dependence. This supposition implies that: (i) the $^4F_{9/2}$ radiative lifetimes for the Dy^{3+} ions in the two sites are nearly the same, and slightly smaller than the calculated radiative lifetime value of 542 µs; (ii) the energy transfer processes among and from the Dy2 sites are more effective than in the Dy1 sites. This may be due to shorter Dy2–O^{2-} bonds, the presence of three non-silicon-bonded atoms (O5) and the occurrence of linear Dy2 chains in the crystal structure.

As concentration increases up to 5 at%, the decays become significantly nonexponential. The time constants of all nonexponential decays were estimated as the mean lifetimes τ_{mean} according to the formula [16]

$$\tau_{mean} = \frac{\int_{t=0}^{\infty} t\, I(t)\, dt}{\int_{t=0}^{\infty} I(t)\, dt} \tag{6}$$

where I is the intensity of luminescence at time t. Strong concentration variations of luminescence intensity from the $^4F_{9/2}$ state point at the presence of energy transfer processes among dysprosium ions at concentrations higher than 1 at%. As a consequence, mean lifetimes decrease from 462 to 107 µs (Dy2 emission) and from 514 to 215 µs (Dy1 emission).

In Fig. 7 the measured luminescence lifetimes are plotted versus temperature. The luminescence decays of the crystals with 1 and 5 at% of dopant were acquired for 21 095 and 17 064 emission lines. It can be seen that temperature insignificantly affects the rates of transitions and the two type

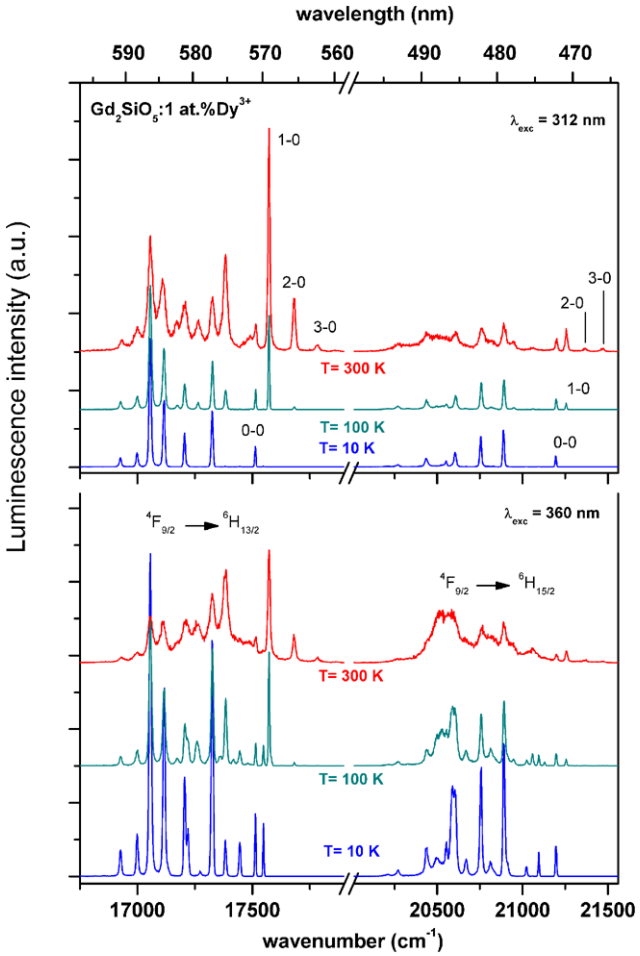

Fig. 5 The temperature dependence of the emission spectra of Dy^{3+}:GSO assigned to $^4F_{9/2} \rightarrow {}^6H_{15/2}$ and $^4F_{9/2} \rightarrow {}^6H_{13/2}$ transitions excited under 312 nm and 360 nm

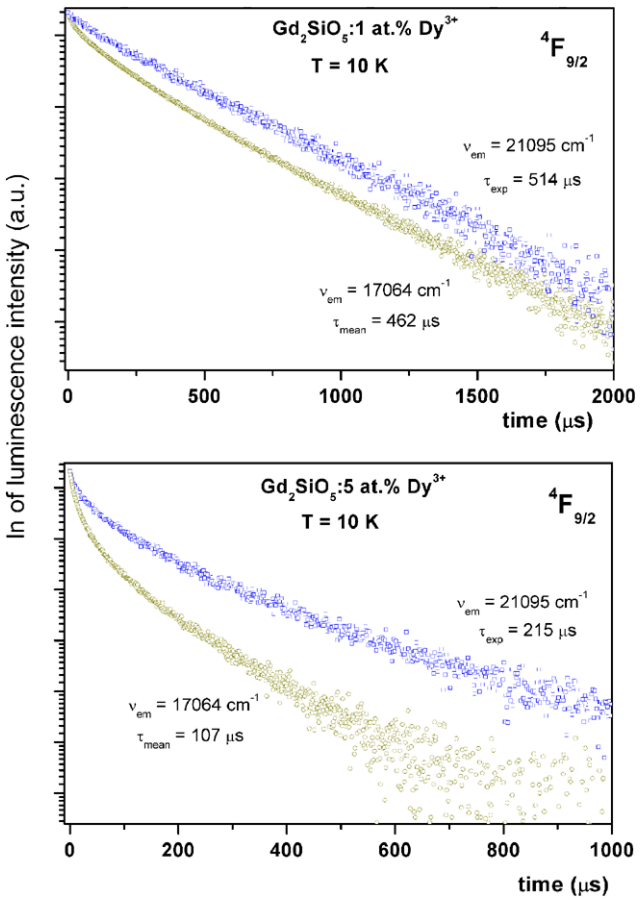

Fig. 6 Decay curves of the $^4F_{9/2}$ luminescence for Gd_2SiO_5 containing 1 and 5 at.% Dy^{3+} recorded in yellow and blue spectral range

of sites decay with dissimilar time constants in the whole temperature region 10–300 K.

3.5 Emission cross-section for the $^4F_{9/2} \rightarrow {}^6H_{13/2}$ transition

One of the most important parameter influencing the potential laser performance of a material is emission cross-section σ_{em} that can be conveniently calculated by the reciprocity method when emission transition from the lowest excited luminescent level to the ground state is considered. Otherwise the Füchtbauer–Ladenburg method is commonly used to estimate this laser parameter. Since the Dy:GSO emission is dominated by the $^4F_{9/2} \rightarrow {}^6H_{13/2}$ transition, the Füchtbauer–Ladenburg method was used to estimate this laser parameter. The dependence between the emission cross-section σ_{em} and emission spectrum is described as [17]

$$\sigma_{em}(\lambda) = \frac{\beta \lambda^5 I(\lambda)}{8\pi n^2 c \tau_{rad} \int \lambda I(\lambda)\, d\lambda} \quad (7)$$

where $I(\lambda)$ represents the experimental emission intensity at the wavelength λ, c is the light velocity, n, β, and τ_{rad} are the refractive index of material, branching ratio, and radiative lifetime of the $^4F_{9/2}$ multiplet, respectively. Figure 8 presents stimulated emission cross-section spectra derived from the $^4F_{9/2} \rightarrow {}^6H_{13/2}$ luminescence of Dy^{3+} excited by the 312- and 360-nm wavelengths and with $n = 1.85$, $\beta = 0.54$, and $\tau_{rad} = 542$ μs. The narrow line at 569.1 nm dominates both emission cross-section spectra. Its maximal value amounts to $\sigma_{em} = 1.21$ (10^{-20} cm^2) when the crystal is excited into the $^6P_{5/2}$ absorption band of Gd^{3+}, and is roughly twice smaller (0.68×10^{-20} cm^2) when dysprosium was excited by the 360 nm wavelength. These values are larger than those of many other materials doped with dysprosium ions. For example, $\sigma_{em} = 0.78$ (10^{-20} cm^2) at 580 nm and 0.37 (10^{-20} cm^2) at 574 nm in Dy:$LiNbO_3$ [18] and Dy:fluoroborate glass [19], respectively. The values of 1.27 (10^{-20} cm^2) at 571 nm was reported for Dy:$YAl_3(BO_3)_4$ [4], whereas $\sigma_{em} = 13$ (10^{-20} cm^2) at 580 nm was found for the $NaGd(WO_4)_2$ crystal [20]. It should be noted here that the calculated σ_{em} values depend on incertitude associated with radiative transition rates derived from a fitting procedure in the framework of the Judd–Ofelt the-

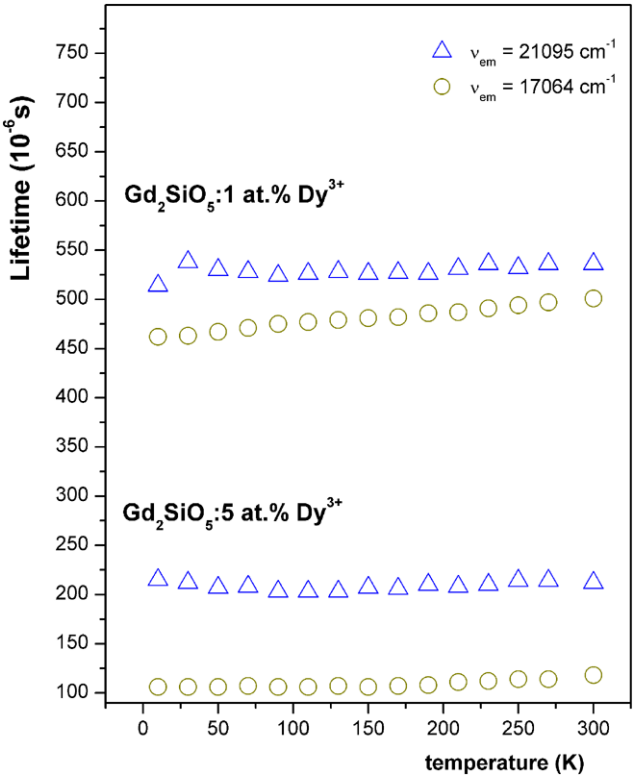

Fig. 7 Temperature dependence of $^4F_{9/2}$ lifetime of Dy^{3+} in Gd_2SiO_5: 1 at% Dy^{3+} and Gd_2SiO_5: 5 at% Dy^{3+} detected at $\nu_1 = 17\,064\ cm^{-1}$ and $\nu_2 = 21\,095\ cm^{-1}$

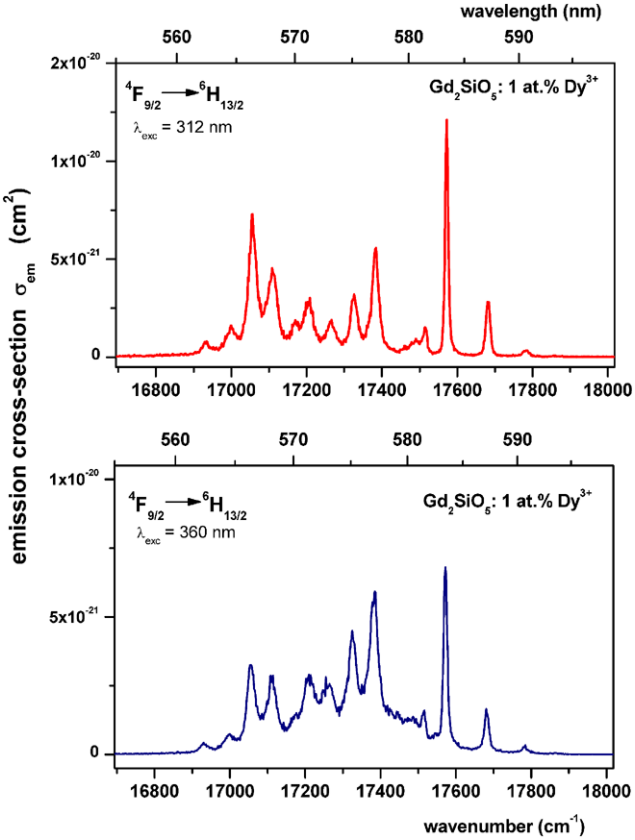

Fig. 8 Emission cross-section spectra for $^4F_{9/2} \rightarrow {}^6H_{13/2}$ transition of dysprosium in Gd_2SiO_5 estimated for the spectra acquired utilizing excitation wavelengths at 312 and 360 nm

ory. Thus, the calculated emission cross-sections should be treated as estimated values to be verified by laser experiments.

4 Conclusions

The spectroscopic characteristics and excited state relaxation dynamics of Dy^{3+} in the Gd_2SiO_5 host were studied. The combination of low-temperature absorption and emission data allowed us to determine the crystal-field components of dysprosium multiplets occupying two crystallographic sites in the host. Moreover, luminescence spectra acquired at 10 K under excitation into Gd^{3+} or Dy^{3+} absorption bands disclosed that the Gd^{3+}–Dy^{+3} energy transfer is very efficient, and only one of two dysprosium sites is evidently preferred by this process. Kinetics studies revealed that luminescence decays of both dysprosium sites are different. The combination of the structural consideration and the optical results with the $^4F_{9/2}$ luminescence dynamics data provided knowledge on spectroscopic properties of the individual dysprosium site and allowed for the site identification. Thus, Dy site characterized by exponential decay of luminescence, and negligible efficiency of the Gd^{3+}–Dy^{+3} energy transfer was identified as the Dy1 site (CN = 9, C_{3v} point symmetry). The Dy site, which is effectively engaged into the energy transfer from excited Gd^{3+} ion, was identified as the Dy2 site (CN = 7, C_s local symmetry).

Based on the presented results, we can conclude that the intense visible luminescence, narrow optical lines, long lifetime of the $^4F_{9/2}$ luminescent level, and higher emission cross-sections for the $^4F_{9/2} \rightarrow {}^6H_{13/2}$ transition are advantageous for the low-threshold laser operation.

Acknowledgements The work was supported by Polish Ministry of Science and Information Society Technologies within a grant 4520/B/T02/2008/34 2008–2010.

References

1. L.F. Johnson, H.J. Guggenheim, Appl. Phys. Lett. **23**, 96 (1973)
2. P.Y. Tigreat, J.L. Doualan, R. Moncorgé, B. Ferrand, J. Luminesc. **94–95**, 107 (2001)
3. P. Babu, K.H. Jang, E.S. Kim, L. Shi, H.J. Seo, F. Rivera-Lopez, U.R. Rodriguez-Mendoza, V. Lavin, R. Vijaya, C.K. Jayasankar, L. Rama Moorthy, J. Appl. Phys. **105**, 013516 (2009)
4. G. Dominiak-Dzik, P. Solarz, W. Ryba-Romanowski, E. Beregi, L. Kovács, J. Alloys Compd. **359**, 51 (2003)
5. K. Takagi, T. Fukazawa, Appl. Phys. Lett. **42**, 43 (1983)
6. Y. Chen, B. Liu, Ch. Shi, M. Kirm, M. True, S. Vielhauer, G. Zimmerer, J. Phys.: Condens. Matter **17**, 1217 (2005)

7. W. Li, H. Pan, L. Ding, H. Zeng, W. Lu, G. Zhao, C. Yan, L. Su, J. Xu, Appl. Phys. Lett. **88**, 221117-1 (2006)
8. R.A. Young, J. Appl. Crystallog. **28**, 366 (1995)
9. M.P. Dramicanin, V. Jokanovic, B. Viana, E. Antic-Fidancev, M. Matric, Z. Andric, J. Alloys Compd. **424**, 213 (2006)
10. A.S. S de Camargo, M.R. Davolos, L.A.O. Nunes, J. Phys.: Condens. Matter **14**, 3353 (2002)
11. W.T. Carnal, H. Crosswhite, H.M. Crosswhite, Energy level structure and transition probabilities in the spectra of the trivalent lanthanides in LaF_3, Argon National Laboratory Report (1997)
12. C.K. Jayasankar, E. Rukmini, Physica B **240**, 273 (1997)
13. G. Dominiak-Dzik, W. Ryba-Romanowski, M.N. Palatnikov, N.V. Sidorov, V.T. Kalinnikov, J. Mol. Struct. **704**, 139 (2004)
14. Y. Zong, G. Zhao, Ch. Yan, X. Xu, L. Su, J. Xu, J. Cryst. Growth **294**, 416 (2006)
15. E. Cavalli, M. Bettinelli, A. Belletti, A. Speghini, J. Alloys Compd. **341**, 107 (2002)
16. M. Inokuti, F. Hirayama, J. Chem. Phys. **43**, 1978 (1965)
17. S.A. Payne, L.L. Chase, L.K. Smith, W.L. Kway, W.F. Krupke, IEEE J. Quantum Electron. **28**, 2619 (1999)
18. M. Malinowski, P. Myziak, R. Piramidowicz, I. Pracka, T. Łukasiewicz, B. Surma, S. Kaczmarek, K. Kopczyński, Z. Mierczyk, Acta Phys. Pol. A **90**, 181 (1996)
19. A.A. Kaminskii, H.J. Eichler, K. Ueda, N.V. Klassen, B.S. Redkin, L.E. Li, J. Findeisen, D. Jaque, J. Garcia-Sole, J. Fernandez, R. Balda, Appl. Opt. **38**, 4533 (1999)
20. H. Wang, J. Li, G. Jia, Z. You, F. Yang, Y. Wei, Y. Wang, Zh. Zhu, X. Lu, Ch. Tu, J. Lumin. **126**, 452 (2007)